Supplementary Information

CONTINUOUS FLOW PHOTOOXYGENATION WITH ADVANCED ROSE BENGAL-ANCHORED POLYMER COLLOIDS

Axelle DESRIAC[§], Guillaume MAGESTE[‡], Mickael LE BECHEC[‡], M. Ali ABOUDZADEH[‡], Thierry PIGOT[‡], Maud SAVE[‡], Jean-François BLANCO[§], Patrice BACCHIN[§], Karine LOUBIERE*[§]

[§] Université de Toulouse, Toulouse INP, CNRS, LGC, Toulouse, France.

[‡] CNRS, Université de Pau et des Pays de l'Adour, E2S UPPA, Institut des Sciences Analytiques et de Physico-Chimie pour l'Environnement et les Matériaux, IPREM, UMR5254, 64000, Pau.

Corresponding Author

* Karine LOUBIERE, Email : karine.loubiere@cnrs.fr

Table of contents

S.0 Nomenclature

Symbol	Meaning	Unit
A	Absorbance	(-)
a	Interfacial area	m^{-1}
a_f	Interfacial area related to the lubrication film between the bubble and the tubing wall	m^{-1}
a_c	Interfacial area related to the bubble's caps	m^{-1}
a_{light}	Specific irradiated surface (Eq.3)	m^2
C_{asc}	Concentration in ascaridole	$mol.L^{-1}$
$C_{\alpha T}$	Concentration in α-terpinene	$mol.L^{-1}$
$C_{\alpha T,0}$	Initial concentration in α-terpinene	$mol.L^{-1}$
C_{O_2}	Concentration in dissolved oxygen	$mol.L^{-1}$
$C_{O_2}^*$	Concentration in dissolved oxygen at saturation	$mol.L^{-1}$
C_{RB}	Concentration in Rose Bengal	$\mu mol_{RB}.L^{-1}$
$C_{RB,0,dispersion}$	Concentration in Rose Bengal inside the initial colloidal suspension (before dilution)	$\mu mol_{RB}.L^{-1}$
$C_{w,polymer,0}$	Weight concentration of polymer inside the dispersion after synthesis	$g.L^{-1}$
$C_{w,polymer}$	Weight concentration of polymer after dilution for flow experiments or for measurements of absorbance	$g.L^{-1}$
d	Inner diameter of the reactor's tubing	m
D_h	Hydrodynamic diameter of the colloid (Table 1)	nm
E	Enhancement factor (Eq. S22)	(-)
ϵ_L	Liquid retention (Eq. S17)	(-)
f	Oxygen/α-terpinene ratio (Eq. S3)	(-)
$F_{\alpha T}$	Molar flow rate of α-terpinene (Eq. S3)	$mol.s^{-1}$
F_{O_2}	Molar flow rate of oxygen (Eq. S3)	$mol.s^{-1}$
F_A	Fraction of absorbed photons	(-)

F_T	Fraction of transmitted photons	(-)
k	Constant in (Eq.8 and S23)	$mol^{-n}.mol_{h\nu}^{-1}$. $mol^{-(2+3n)}$
l	Characteristic optical path length	mm
L_b	Length of a bubble (Fig. S14)	m
L_{uc}	Unit Cell length (Fig. S13)	m
M_{air}	Molar mass of air	$g.mol^{-1}$
n	Order of the reaction	(-)
N_{slug}	Number of slugs, or bubbles (Eq. S17)	(-)
PDI	Polydispersity index (Table 1)	(-)
q_0	Incident photon flux density (Eq. 3)	$mol_{h\upsilon}.m^{-2}.s^{-1}$
q_r	Photon flux density arriving at the outer surface of the reactor	$mol_{h\upsilon}.m^{-2}.s^{-1}$
Q_G	Air volumetric flow rate	$L.min^{-1}$
Q_L	Liquid volumetric flow rate	$L.min^{-1}$
RB loadings	Experimental molar loading of RB in the colloid (Table 1)	$\mu mol_{RB}.g_{polymer}^{-1}$
R_Q	Volumetric ratio (Eq. 1)	(-)
$S_{asc/aT}$	Selectivity of the reaction (Eq. S8)	(-)
S_c	Surface related to the bubble's caps (Eq. S15)	m^2
S_f	Surface related to the lubrication film between the bubbles and the walls (Eq. S14)	m^2
V_G	Gas volume related to the bubble's caps (Eq. S17)	m^3
V_L	Liquid volume (Eq. S17)	m^3
V_{slug}	Slug volume (Eq. S17)	m^3
V_{uc}	Unit cell volume (Eq. S13)	m^3
V_R	Reactor volume	L
Γ_0	Initial rate of the photooxygenation reaction	s^{-1}

$\varepsilon_{\lambda_{max}}$	Molar absorption coefficient at maximum absorption wavelength	L.mol^{-1}.cm^{-1}
η_{asc}	Yield of ascaridole	(-)
λ_{max}	Wavelength at which absorption is maximum for S2 band (section 7)	nm
τ	Residence time defined as $V_R/(Q_G + Q_L)$	s
ϕ	Overall quantum yield (Eq. 3)	$mol.mol_{h\nu}^{-1}$
ρ	Reflectivity coefficient of the plate's material (Eq. 3)	(-)
ρ_{air}	Density of air at the working temperature	g.L^{-1}
$\chi_{\alpha T}$	Conversion in α-terpinene	(-)
χ_{RB}	Photobleaching yield	(-)

S.1 Chemicals and benchmark reaction

Rose Bengal sodium salt (CAS: 632-69-9; purity ≥ 95 %; 1017 g.mol^{-1}; Sigma-Aldrich), α-terpinene (CAS: 99-86-6; purity ≥ 89 %; 136.17 g.mol^{-1}; Sigma-Aldrich), p-cymene (CAS: 99-87-6; purity 99 %, 134.22 g.mol^{-1}; Sigma-Aldrich), eucalyptol (CAS: 470-82-6; 99 %, 154.25 g.mol^{-1}, Sigma-Aldrich), dodecane (CAS: 112-40-3; ≥ 99 %, 170.33 g.mol^{-1}, Sigma- Aldrich) were used in solution with the same ethanol than the one used for synthetizing the photoactive colloids (CAS: 64-17-5; purity = 96 %; 46.07 g.mol^{-1}; Sigma-Aldrich). The commercial α-terpinene contained two primary impurities: p-cymene (~2 % by mass) and eucalyptol (~8 % by mass), along with other unidentified minor species (~1 % by mass).

Figure S1: Synthesis of ascaridole from α-terpinene with the presence of two main by-products: p-cymene and eucalyptol.

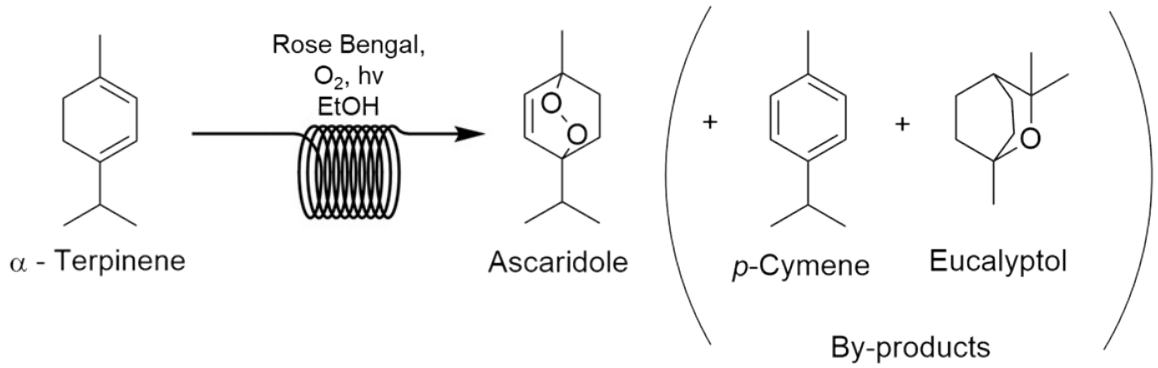

S.2 Feature of core-shell polymer colloids: information on synthesis, structure of polymers and characterization methods

The core-shell latex particles covalently linked with Rose Bengal photosensitizer (noted RB@CSLP$_{x/y}$) reported in **Table 1** were synthesized by surfactant-free reversible addition fragmentation transfer (RAFT) dispersion polymerization in ethanol. The block copolymers are made from a first solvophilic polymer block composed of a statistical poly(oligo(ethylene glycol) methacrylate-co-ethyl methacrylate Rose Bengal) P(OEGMA-co-EMARB), which acted as stabilizer of particles, and a second poly(benzyl methacrylate) PBzMA solvophobic block chain extended by RAFT dispersion polymerization in ethanol from the first reactive block. The self-assembly of solvophilic/solvophobic P(OEGMA-co-EMARB)-b-PBzMA block copolymer intrinsically produce the core-shell morphology to the latex particles (**Figure S2**). The synthesis of the core-shell particles is based on the know-how already developed by the co-authors for other core-shell latex particles synthesized by emulsion polymerization in water.[1] This approach was adapted for synthesis of CSLP by dispersion polymerization in ethanol, and the corresponding detailed work on synthesis and determination of quantum yield of singlet oxygen will be published soon by some of us.

The experimental loading of RB per weight of polymer is calculated by UV-visible spectroscopy from **Table 1.**

$$\text{RB Loading } (\mu\text{mol.g}_{\text{polymer}}^{-1}) = \frac{C_{RB}}{C_{\text{wt, polymer}}} = \frac{A_{\lambda_{max}}}{C_{\text{wt, polymer}} \times \varepsilon_{\lambda_{max}} \times l} \quad (Eq.\ S1)$$

$C_{\text{wt,polymer}}$ (g.L^{-1}) is the weight concentration of polymer in the UV-visible cuvette after dilution form the initial latex suspension, l is the cuvette length of 1 cm, $A_{\lambda max}$ is the absorbance at the

maximum wavelength of S2 band reported in **Table S8** (section S7) and $\varepsilon_{\lambda_{max}}$ the related absorption coefficient (see section S6).

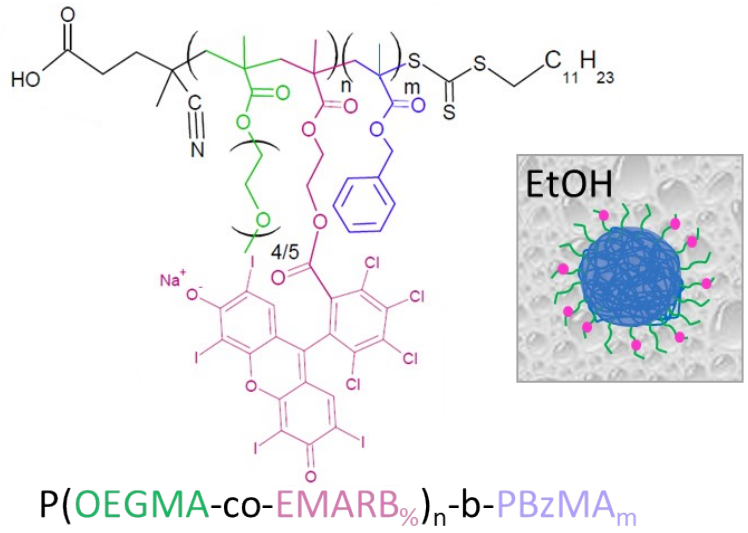

Figure S2 : Structure of P(OEGMA-co-EMARB)-b-PBzMA block copolymers forming the core-shell latex particles (CSLP) synthesized by RAFT dispersion polymerization in ethanol. *n* and *m* correspond to the degree of polymerization (DP = number of monomer units) of each polymer block (see **Table S1**).

The weight concentration of polymer per volume of the total dispersion after synthesis, $C_{w,polymer,0,}$ can be defined as:

$$C_{w,polymer,0}\ (g.L^{-1}) = \frac{m_{polymer}}{V_{polymer} + V_{ethanol}} \qquad (Eq.\ S2)$$

The measurements of the hydrodynamic diameter D_h and polydispersity index in brackets [PDI] reported in **Table 1** were carried out at room temperature in ethanol for a colloid

concentration of 0.5 g.L^{-1} on a Nano-ZS, Model ZEN3600 (Malvern, UK) zetasizer. A He-Ne 4.0mW power laser was used, operating at a wavelength of 633 nm and an angle of 173°. For evaluation of the data, the DTS (Nano) program was used. The non-negative least square (NNLS) method was used to provide average values of hydrodynamic diameters (D_h), the polydispersity (PDI) was excreted from the cumulant mode.

The photosensitizer loading onto the core-shell latex particles was determined from their UV-visible absorbance spectra, assuming the same molar absorption coefficients of both supported RB (noted RB@CSLP$_{x/y}$) and soluble RB at their respective maximum absorption wavelengths (570 nm vs 557 nm, see section S4), namely that:

$\varepsilon_{RB@CSLP,\ 570\ nm} = \varepsilon_{soluble\ RB,\ 557\ nm} = 108\ 000 \pm 3000$ L.mol^{-1}.cm^{-1}.

Table S1: Main features of the core-shell latex particles anchoring Rose Bengal in the outer shell (RB@CSLP$_{x/y}$)

Nomenclature of Table 1 [a]	Detailed nomenclature for block copolymers [b]	$C_{w,polymer,0}$ [c] (g.L^{-1})
RB@CSLP$_{66/2.0}$	P(OEGMA-co-EMARB$_{0.22\ \%}$)$_{58}$-b-PBzMA$_{188}$	141
RB@CSLP$_{112/1.1}$	P(OEGMA-co-EMARB$_{0.22\ \%}$)$_{58}$-b-PBzMA$_{348}$	210
RB@CSLP$_{122/2.1}$	P(OEGMA-co-EMARB$_{0.44\ \%}$)$_{43}$-*b*-PBzMA$_{375}$	70
RB@CSLP$_{162/3.4}$	P(OEGMA-co-EMARB$_{0.90\ \%}$)$_{39}$-*b*-PBzMA$_{632}$	103
RB@CSLP$_{167/0.68}$	P(OEGMA-co-EMARB$_{0.19\ \%}$)$_{39}$-b-PBzMA$_{589}$	75
RB@CSLP$_{257/0.21}$	P(OEGMA-co-EMARB$_{0.19\ \%}$)$_{39}$-b-PBzMA$_{1170}$	138

[a] In the RB@CSLP$_{x/y}$ code of polymer colloids, *x* corresponds to the hydrodynamic diameter of the core-shell particle and *y* to the experimental molar RB loading per gram of polymer ($\mu mol_{RB}.g_{polymer}^{-1}$) (Eq. S1) as reported in **Table 1**.

[b] The block copolymer codes are as follows: P(OEGMA-co-EMARB$_{F_EMARB_mol\%)_n}$-b-PBzMA$_m$ with F_{EMARB} the experimental molar fraction of EMARB (in mol %,) in the P(OEGMA-co-EMARB$_{F_EMARB_mol\%)_n}$ first block, n and m the degree of polymerization (DP = number of monomer units) of each polymer block determined by size exclusion chromatography.

[c] $C_{w,polymer,0}$ corresponds to the weight concentration of polymer in the dispersion after synthesis (see Eq. S2).

S.3 Implementation of the Gas-liquid Taylor flows

The liquid phase pumping system consisted of a high-pressure syringe pump (neMESYS High-Pressure Module, Cetoni®; syringe volume: 25 or 50 mL) made of stainless steel. The air flow rates were controlled using two Brooks (model: SLA 5800 series) mass flow controller with two maximum flow rates: 3 and 30 $mL.min^{-1}$. Air was supplied from the high-pressure air network of the laboratory and a pressure gauge enabled to set the pressure at 2 bars. The outlet of the reactor operated at atmospheric pressure (no back-pressure system). A perfluoroalkoxy (PFA) T-junction with an internal diameter of 1 mm was used to introduce gas bubbles into the liquid flow to produce regular bubbles and liquid slugs. Under these conditions, stable and regular Taylor flows were achieved over all the reactor's length, as illustrated in **Figure S3**. The liquid flow rate ranges from 0.11 to 1.99 $mL.min^{-1}$ and the gas flow rate ranges from 0.58 to 6.81 $mL.min^{-1}$. Note that the pressure drop in this reactor was quantified, without colloids, in a previous work:[2] they were measured from 0.15 to 0.25 bar per tube meter for Reynolds numbers (defined from the two-phase superficial velocity) ranging from 50 to 200.

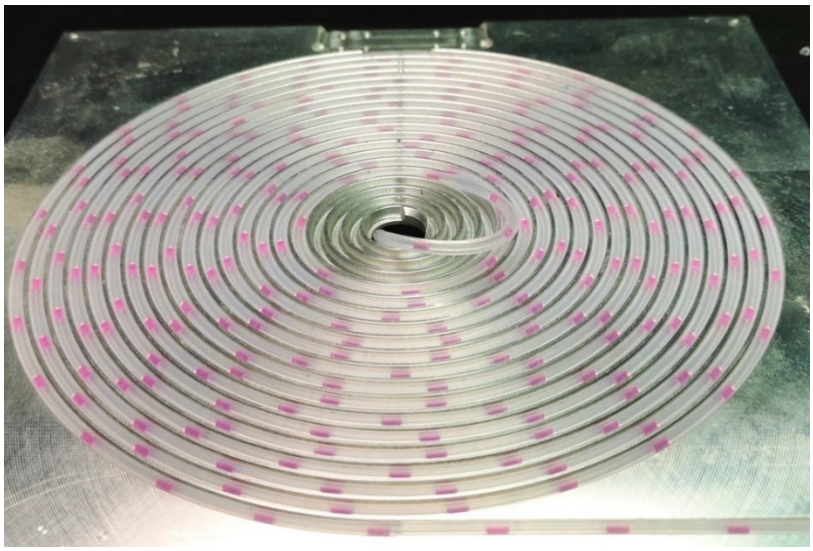

Figure S3: Typical image of gas-liquid Taylor flows with soluble RB obtained in the spiral-shaped microreactor (volumetric ratio R_Q equal to 4.2)

The oxygen/α-terpinene ratio, *f*, was defined as:

$$f = \frac{F_{O_2}}{F_{\alpha T}} \qquad (Eq.S3)$$

where F_{O_2}, mol.s^{-1}, was the molar flow rate of oxygen contained in the bubbles at the inlet of the reactor and, and $F_{\alpha T}$, mol.s^{-1}, the one of α-terpinene, $F_{\alpha T}$, calculated from the initial concentration in α-terpinene inside the syringe, $C_{\alpha T,0}$ (mol.L^{-1}) :

$$F_{\alpha T} = C_{\alpha T,0} \times Q_L \qquad (Eq.S4)$$

And, F_{O_2} was calculated assuming air as perfect gas.

$$F_{O_2} = \left(\frac{0.21 \times \rho_{air}}{M_{air}} \right) \times Q_G \qquad (Eq.S5)$$

With M_{air} (g.mol^{-1}) the molar mass of air (28.97 g.mol^{-1}) and ρ_{air} (g.L^{-1}) the density of air at the working temperature.

S.4 LED array: emission spectrum and radiant power

The same LED panel than the one in our previous work[3] was used for this study. Placed at a distance of 20 cm from the surface of the spiral-shaped reactor, the LED panel was controlled by a Labview® software, which also enabled real-time monitoring of the LED temperature, tuning the emitted radiant power and selecting a specific spectral domain between 400 nm and 700 nm.

Figure S4 presents the spectral distribution of the radiant energy flux density (given by the manufacturer) for the mode used in this study (referred as "yellow mode" in our present work[4] in which actinometry measurements with Reinecke's salt were reported and modelled). One should note that, as the LED panel was equipped with a glass diffuser, the emission could be considered as Lambertian.

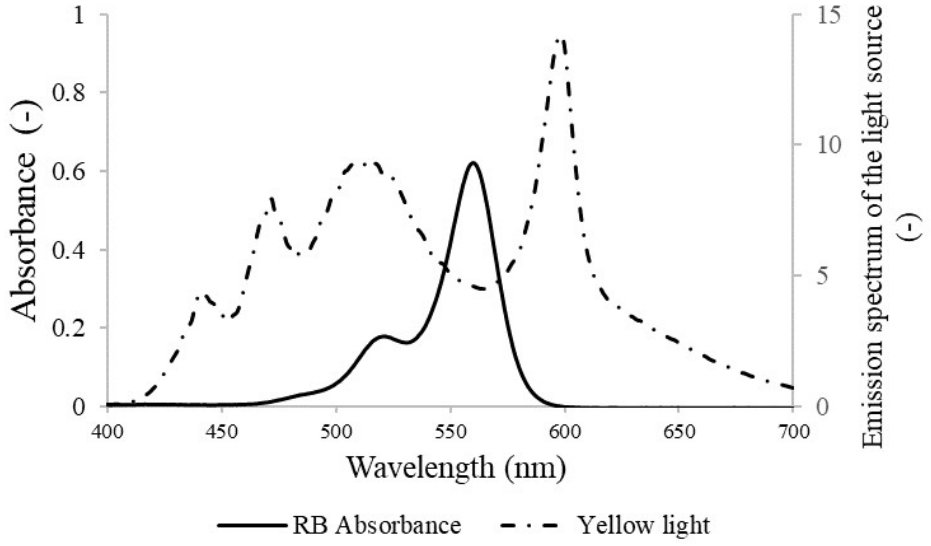

Figure S4: Spectral distribution of the radiant energy flux density measured (by the manufacturer) at 20 cm from the LED array for the mode used in this study (dotted line) and Rose Bengal absorbance spectra at 6 µmol.L^{-1} (plain line)

Photon flux densities used in this study, obtained with different power levels and distances, are shown in **Table S2**. They were deduced from measurements with the Quantum Sensor (LI-190R-BNC-5 sensor from LI-COR®, equipped with a LI-250A Light meter) positioned at different locations onto the microreactor's surface, as described in our previous work.[3] Note that they are measured in the P.A.R range (e.g. between 400 and 700 nm), while the RB absorbs only between 400 and 600 nm (see **Figure S4**).

Table S2: Averaged photon flux densities q_r measured at the surface of the milli-reactor by the LI-COR quantum sensor, for different levels of emitted power.

Level Distance	q_r ($\mu mol_{h\upsilon}.m^{-2}.s^{-1}$) *From the LI-COR sensor* [Min – Max]	q_r ($mW.cm^{-2}$) *From the LI-COR sensor*
Minimun 20 cm	976 [845 – 1066]	22
Low 20 cm	1668 [1440 – 1821]	37

S.5 Conversion, yield and selectivity of the reaction

The concentration in α-terpinene was monitored, at the microreactor's outlet, by GC-FID measurements. GC analysis were performed on a TRACE™ 1310 from ThermoFisher Scientific, equipped with an auto-injector AI3000 using the Chromeleon 7.2 software with a controlled method (carrier gas: He; injector: Temperature = 200 °C; split ratio = 50:1; oven program: 50 °C (1 min) – 250 °C (1 min) at 15.4°C.min^{-1}; FID detector (Temperature = 280 °C, no make-up gas); injection volume: 1 µL). The column used was a Phenomenex Zebron™ ZB-5 low polarity (0.25 mm ID × 0.25 µm film thickness × 30 m length).

The internal standard used in this study was dodecane at 0.4 g.L^{-1} in each sample.

The response factors, defined as the inverse of the slope of the calibration curve, for ascaridole, α-terpinene and *p*-cymene are respectively 1.67 ± 0.02, 1.03 ± 0.01 and 0.91 ± 0.01. Those

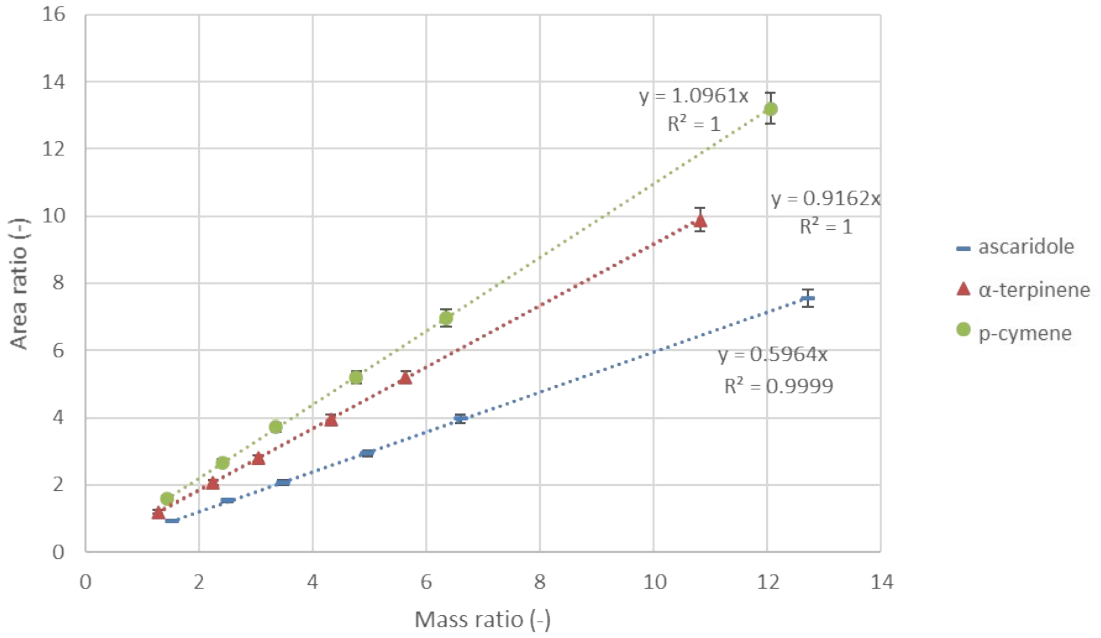

calibration curves are presented in **Figure S5**.

Figure S5 : Calibration curve for α-terpinene, p-cymene and ascaridole with dodecane as internal standard (for 2 mg of dodecane in 5 mL)

The conversion of α-terpinene was defined according to

$$\chi_{\alpha T} = \left(1 - \frac{C_{\alpha T,\tau}}{C_{\alpha T,0}}\right) \times 100 \qquad (Eq.\,S6)$$

where $C_{\alpha T,\tau}$ is the concentration in α-terpinene at the outlet of the spiral-shaped reactor for a residence time τ, and $C_{\alpha T,0}$ is the initial concentration in α-terpinene.

In addition, the percentage of by-products (p-cymene and eucalyptol) was systematically measured to compare the conversion of α-terpinene with the yield in ascaridole, defined as the ratio between the formed moles of ascaridole to the initial moles of α-terpinene (see Eq. S7).

For all the experiments, the reaction medium contained ascaridole, p-cymene, eucalyptol, eventually α-terpinene if the conversion was not complete, and other non-identified components (above 6 min), as illustrated in **Figure S6**.

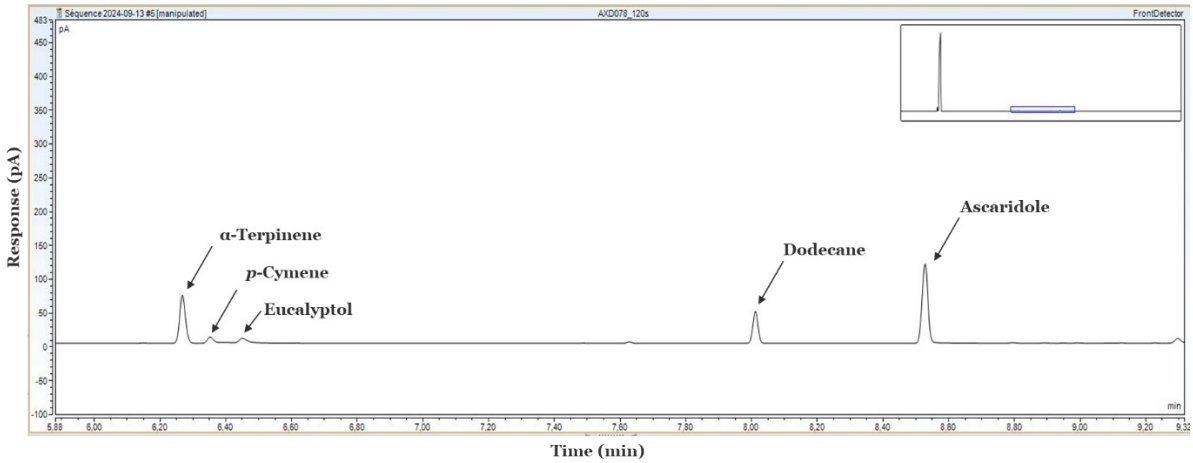

Figure S6: Standard chromatogram related to a sample collected at the outlet of the LED-driven spiral shaped-microreactor for a residence time of 120 s ($\chi_{\alpha T}$ = 72 %, $S_{asc/\alpha T}$ = 82 %, $C_{\alpha T,0} = 3.10^{-2}$ mol.L^{-1}; R_Q= 3 ± 0.06 ; f = 1.21 ± 0.02; q_r= 1668 µmol$_{h\upsilon}$.m^{-2}.s^{-1})

The yield of ascaridole was defined according to

$$\eta_{asc} = \frac{C_{asc,\tau}}{C_{\alpha T,0}} \times 100 \qquad \text{(Eq. S7)}$$

where $C_{asc,\tau}$ is the concentration in ascaridole at the outlet of the spiral-shaped reactor for a residence time τ.

The selectivity was calculated following

$$S_{asc/\alpha T} = \frac{\eta_{asc}}{\chi_{\alpha T}} \times 100 \qquad \text{(Eq. S8)}$$

For all the photooxygenation experiments, it was shown that the conversion of α-terpinene could be considered close to the yield of ascaridole. This demonstrated good selectivity of the reaction studied (see **Table S3, S4, S5, S6**, **S9, S10, S11, S12**).

S.6 Photobleaching yield

The changes in absorbance of the reaction medium (i.e. the photobleaching yield, χ_{RB}) were monitored by considering the intensity of the S2 peak corresponding to the wavelengths noted λ_{max} (see **Figure S8**).

Soluble RB: To ensure good spectrophotometric monitoring, a calibration curve with soluble RB was performed at λ_{max}=557 nm to determine the actual molar extinction coefficient (ε) of the RB (**Figure S7**). In our case, it was found equal to

$$\varepsilon_{soluble\ RB, \lambda_{max}} = 108\ 000 \pm 3000\ \text{L.mol}^{-1}.\text{cm}^{-1} \qquad (Eq.\ S9)$$

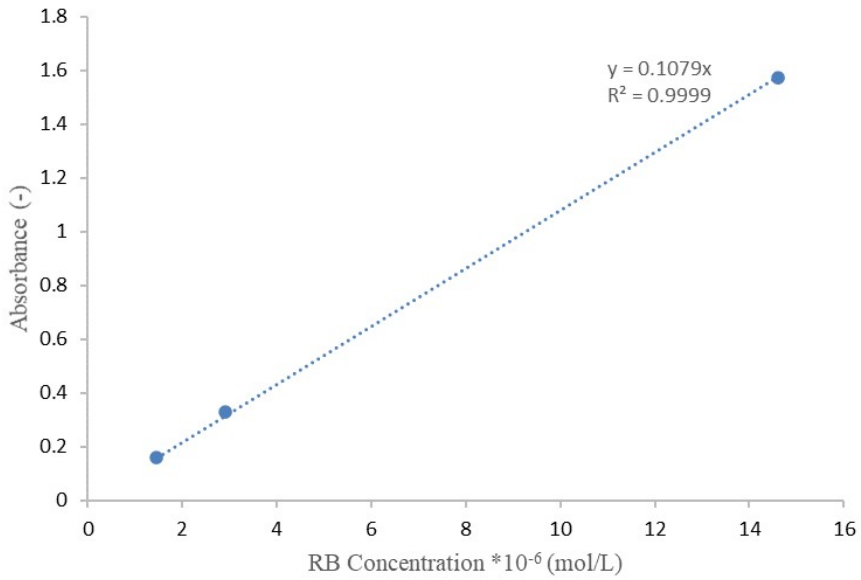

Figure S7: Calibration curve of soluble Rose Bengal in ethanol at 557nm, obtained in a quartz cell with 1 cm of width

The absorbance in the spiral-shaped microreactor could be estimated according to the Beer-Lambert-Bouguer law (Eq. S10)

$$A_{\lambda_{max}} = l \times \varepsilon_{\lambda_{max}} \times C_{RB} \qquad (Eq.\ S10)$$

Where l is the characteristic optical path length assumed equal to the tube's inner diameter (1 mm), For C_{RB} = 0.1, 6 and 12 µmol.L^{-1}, the absorbances were respectively found equal to 0.001, 0.065 and 0.123. They were very low, thus showing that, in the experiments, the medium could be considered as "transparent". A significant part of the incident photons was not absorbed by the RB molecules, thus transmitted over the back optical wall of the microreactor (aluminum plate), and partly reflected.

Photoactive colloids: the molar concentrations of RB have been estimated for each type of colloids knowing the RB loading and mass concentration measurements. To confirm their values, and adjust them if required, a baseline correction was performed as the absorption spectra were distorted due to light scattering by these colloidal objects, as explained in the **Section S7**. Once the spectra corrected, the molar concentration in RB inside the initial colloid stock solutions, $C_{RB,0}$ could be deduced by assuming the same molar extinction coefficient that the one of soluble RB (see Eq. S9) even if a bathochromic shift was occurring. From this knowledge, the stock solutions could be diluted to reach the desired concentration for the experiment, C_{RB}.

Photobleaching yield: χ_{RB}, was calculated, at a given residence time τ,

$$\chi_{RB} = \left(1 - \frac{A_{\lambda_{max,\tau}}}{A_{\lambda_{max},\tau 0}}\right) \times 100 \qquad (Eq.S11)$$

Where $A_{\lambda_{max,\tau 0}}$ (-) and $A_{\lambda_{max,\tau}}$ (-) were the values of absorbance of the reaction medium measured at λ_{max}, at the inlet and at the outlet of the microreactor (*e.g.* after a residence time τ), respectively.

S.7 UV-VIS absorption spectra

The UV-visible absorption spectra were measured using a Shimadzu UV-1800 instrument. As illustrated in the following figures, the absorption spectra of the soluble RB and RB-anchored latex particles in ethanol displayed a maximum at λ_{max} = 557 nm for soluble RB, with a shifted maximum at λ_{max} = 570 nm for all RB colloids. In addition to this peak, named S2, a smaller peak existed, noted S1, which characteristic wavelength was 520 nm for soluble RB and 528 nm for the colloids. Due to the occurrence of light scattering by the latexes, the absorption spectra were distorted, the extent of which depends on the particle sizes and concentrations. In order to accurately determine the Rose Bengal molar concentration for each latex solution under test, a Python program (see **Section S8**) was developed to correct the baseline via exponential regression. Its application is shown in the following figures. Due to too strong light scattering, this baseline correction could not be applied to colloids RB@CSLP$_{167/0.68}$ and

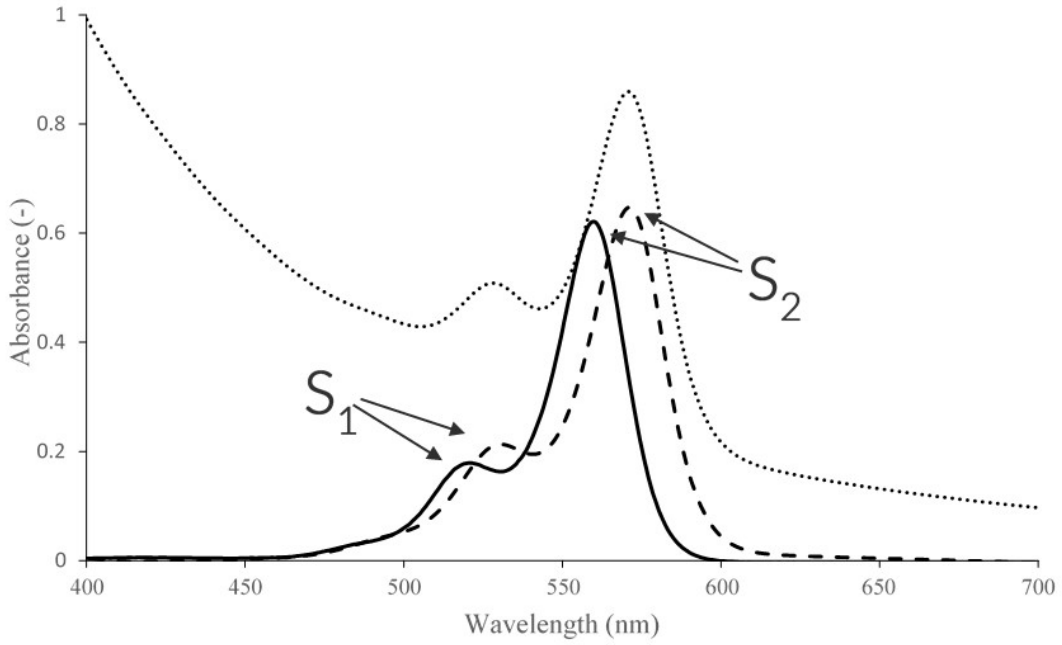

RB@CSLP$_{257/0.21}$.

Figure S8: Absorption spectrum of a free RB solution in ethanol at 6 µmol.L^{-1} (solid line) and of a RB@CSLP$_{122/2.1}$ solution at 2.34 g.L^{-1} before (dotted line) and after (dashed line) baseline correction. Measurement performed in a quartz cell with 1 cm of width and at 25 °C

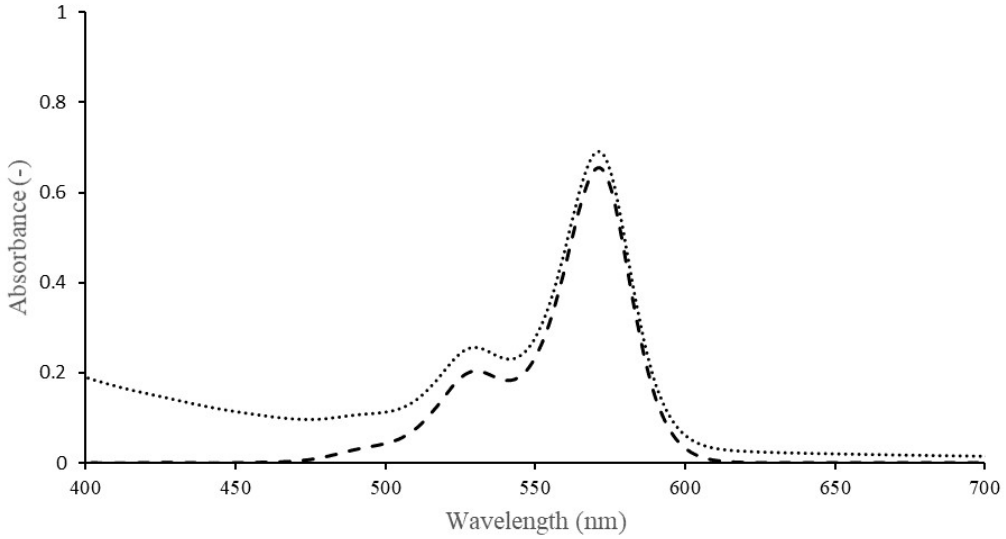

Figure S9: Absorption spectrum of a RB@CSLP$_{66/2.0}$ solution at 2.48 g.L^{-1} before (dotted line) and after (dashed line) baseline correction. Measurement performed in a quartz cell with 1 cm of width and at 25 °C.

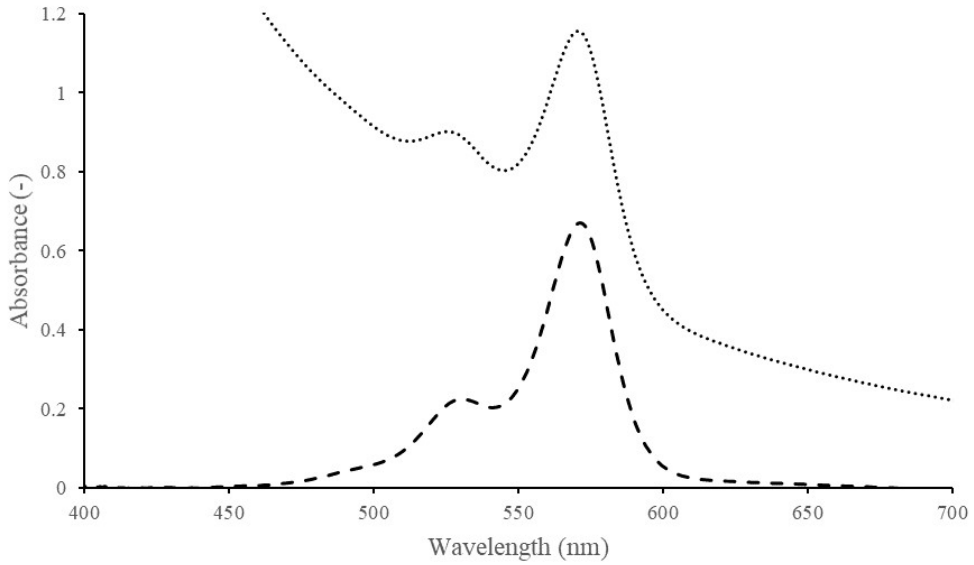

Figure S10 : Absorption spectrum of a RB@CSLP$_{112/1.1}$ solution at 4.42 g.L^{-1} before (dotted line) and after (dashed line) baseline correction. Measurement performed in a quartz cell with 1 cm of width and at 25 °C.

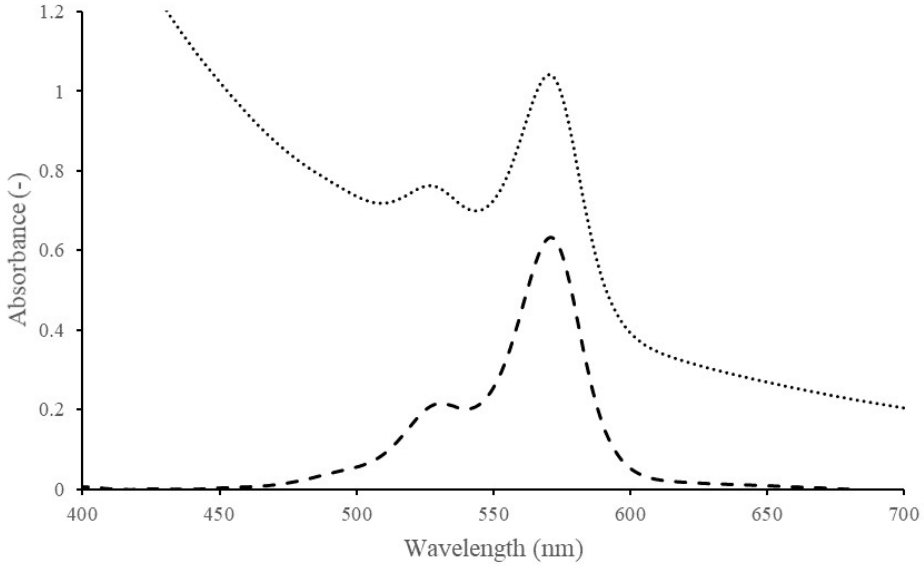

Figure S11: Absorption spectrum of a RB@CSLP$_{162/3.4}$ solution at 1.33 g.L^{-1} before (dotted line) and after (dashed line) baseline correction. Measurement performed in a quartz cell with 1 cm of width and at 25 °C.

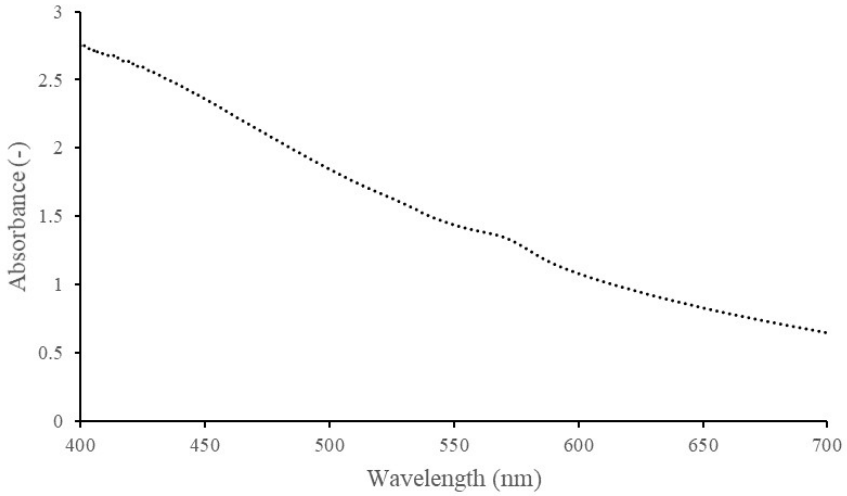

Figure S12: Absorption spectrum of a RB@CSLP$_{257/0.21}$ solution at 5.21 g.L^{-1}. Measurement performed in a quartz cell with 1 cm of width and at 25 °C.

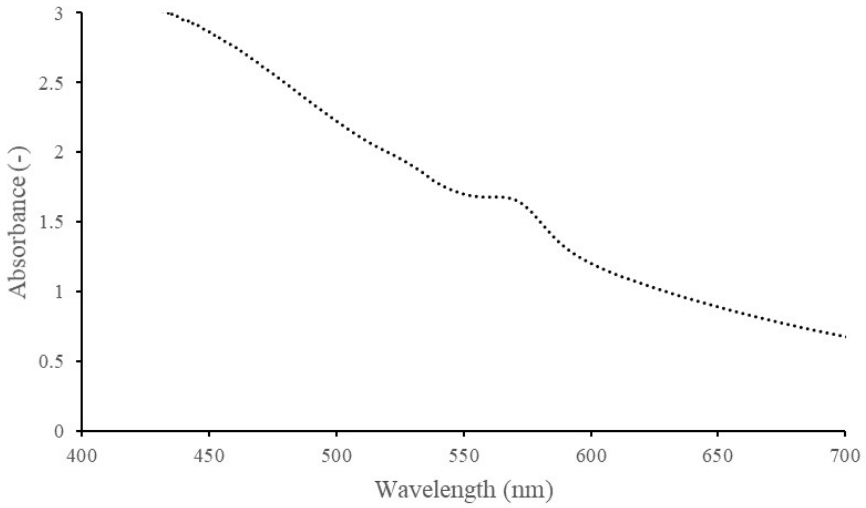

Figure S13: Absorption spectrum of a RB@CSLP$_{167/0.68}$ solution at 3.01 g.L^{-1}. Measurement performed in a quartz cell with 1 cm of width and at 25 °C.

S.8 UV spectrum treatment (Python code)

The code used for UV spectrum treatment (base line subtraction + peak deconvolution) is available below:

https://github.com/bacchin/chemical_engineering_python/blob/master/rech/treatment_spectrum_UV.ipynb

S.9 Tests with blank colloids

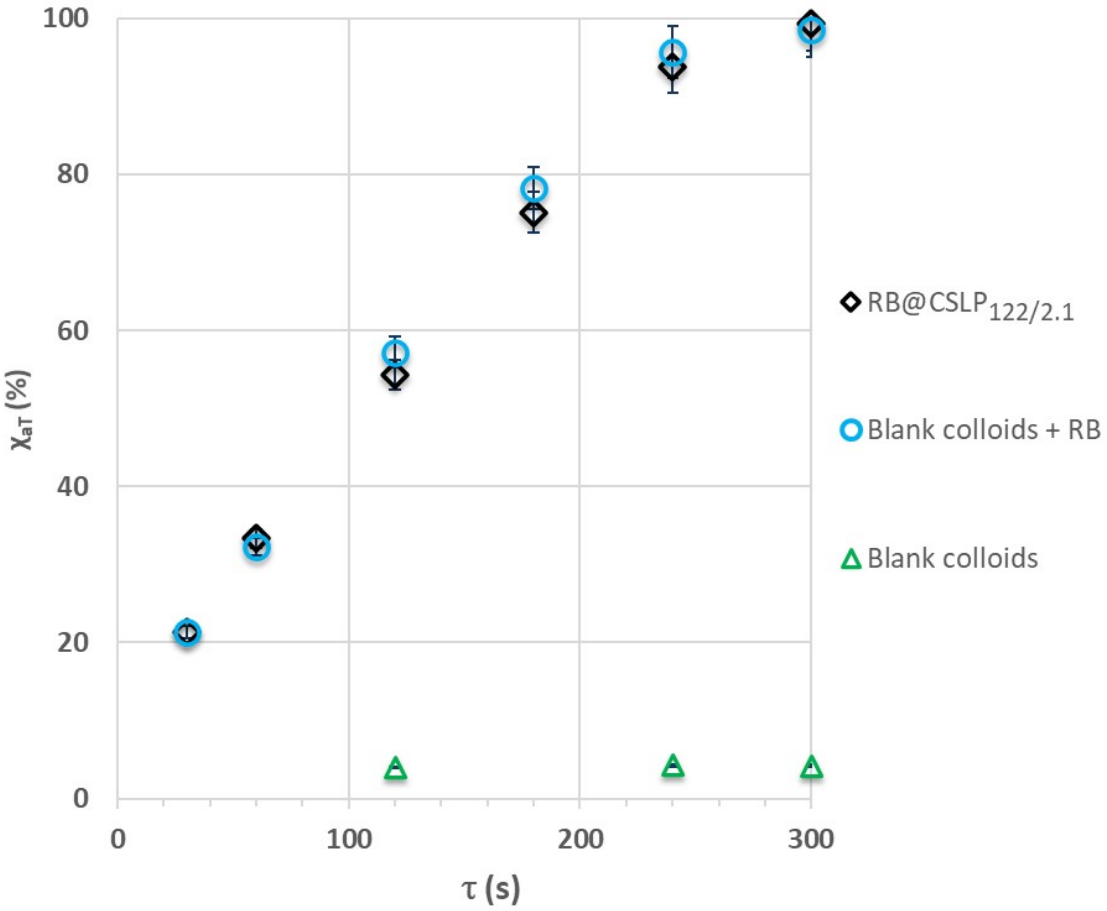

Figure S14: Conversion of α-terpinene, $\chi_{\alpha T}$, versus residence time, τ, for the latex particles RB@CSLP$_{122/2.1}$ (see Table S1), blank colloids (without RB) and RB solubilized in ethanol (operating conditions: C_{RB} = 6.10^{-6} mol.L^{-1}, $C_{\alpha T,0}$ = 3.10^{-2} mol.L^{-1}; R_Q=4.26 ± 0.06 ; f = 1.21 ± 0.02; q_r= 1668 µmol$_{hν}$.m^{-2}.s^{-1})

S.10 Effect of the photon flux density

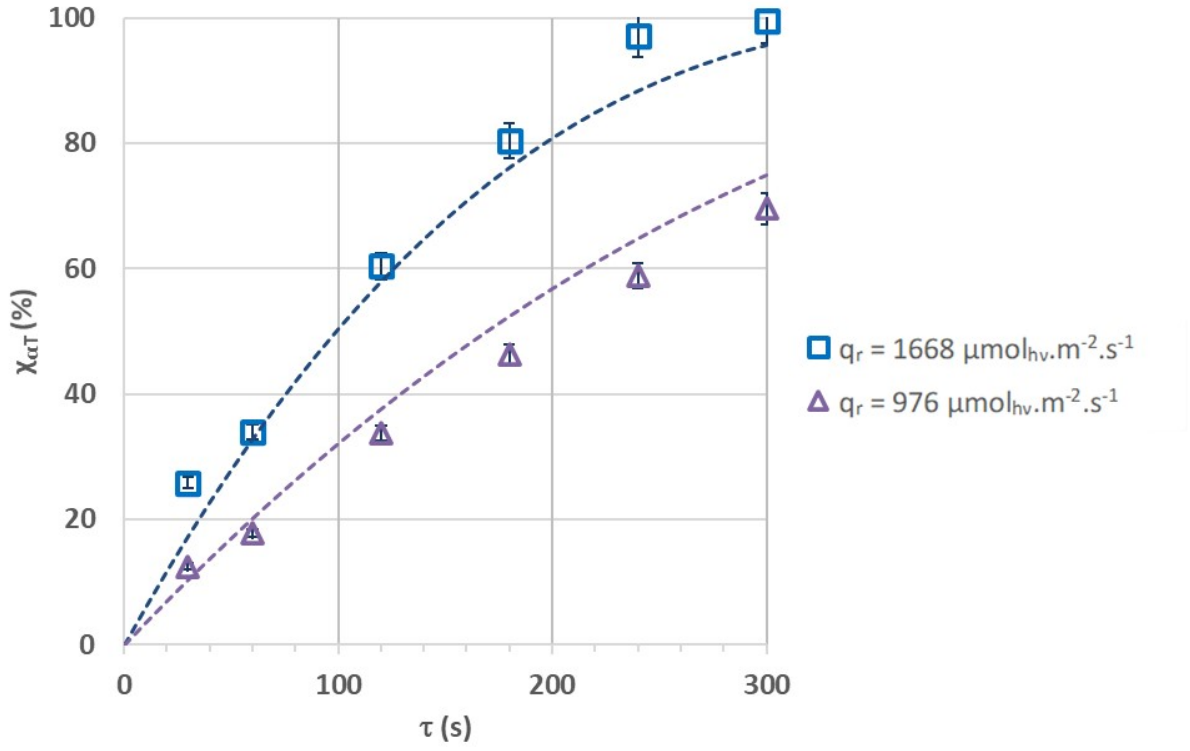

Figure S15: Conversion of α-terpinene, $\chi_{\alpha T}$, versus residence time, τ, for RB solubilized in ethanol for two incident photon flux densities (q_r = 976 and 1668 $\mu mol_{hv}.m^{-2}.s^{-1}$). The conversions predicted by the model (Eq. 9) are shown as dotted lines for each incident photon flux density. Operating conditions: $C_{RB} = 6.10^{-6}$ mol.L^{-1}; $C_{\alpha T,0} = 3.10^{-2}$ mol.L^{-1}; $R_Q = 4.26 \pm 0.06$; $f = 1.21 \pm 0.02$.

Table S3 : Conversion of α-terpinene and yield of ascaridole for different photon flux densities and residences times (see **Figure S15**)

Photon flux density ($\mu mol_{h\upsilon}.m^{-2}.s^{-1}$)	**Conversion (%)**						**Yield (%)**					
	30 s	**60 s**	**120 s**	**180 s**	**240 s**	**300 s**	**30 s**	**60 s**	**120 s**	**180 s**	**240 s**	**300 s**
976	12.5 ± 0.4	17.8 ± 0.6	33.7 ± 1.2	46.7 ± 1.6	58.9 ± 2.1	69.6 ± 2.4	10.5 ± 0.4	15.5 ± 0.5	27.2 ± 1.0	41.7 ± 1.5	50.6 ± 1.8	60.1 ± 2.1
1668	25.8 ± 0.9	34.0 ± 1.2	60.4 ± 2.1	80.5 ± 2.8	97.1 ± 3.4	99.5 ± 3.5	15.8 ± 0.6	27.8 ± 1.0	50.8 ± 1.8	70.2 ± 2.5	86.2 ± 3.0	86.3 ± 3.0

Table S4: Selectivity and photobleaching yield for different photon fluxes and residence times (see **Figure S15**)

Photon flux density ($\mu mol_{h\upsilon}.m^{-2}.s^{-1}$)	**Selectivity**						**Photobleaching yield (%)**					
	30 s	**60 s**	**120 s**	**180 s**	**240 s**	**300 s**	**30 s**	**60 s**	**120 s**	**180 s**	**240 s**	**300 s**
976	84.2 ± 2.9	86.8 ± 3.0	80.7 ± 2.8	90.1 ± 3.1	86.0 ± 3.0	86.4 ± 3.0	3.0 ± 0.1	3.0 ± 0.1	3.0 ± 0.1	3.0 ± 0.1	3.0 ± 0.1	3.0 ± 0.1
1668	61.3 ± 2.1	81.8 ± 2.9	84.1 ± 2.9	87.3 ± 3.1	88.8 ± 3.1	86.8 ± 3.0	5.0 ± 0.1	5.0 ± 0.1	5.0 ± 0.1	3.3 ± 0.1	1.7 ± 0.1	3.3 ± 0.1

S.11 Effect of the volumetric ratio R_Q

S.11.a *Effect of the volumetric ratio on the photoxygenation's perfomances.*

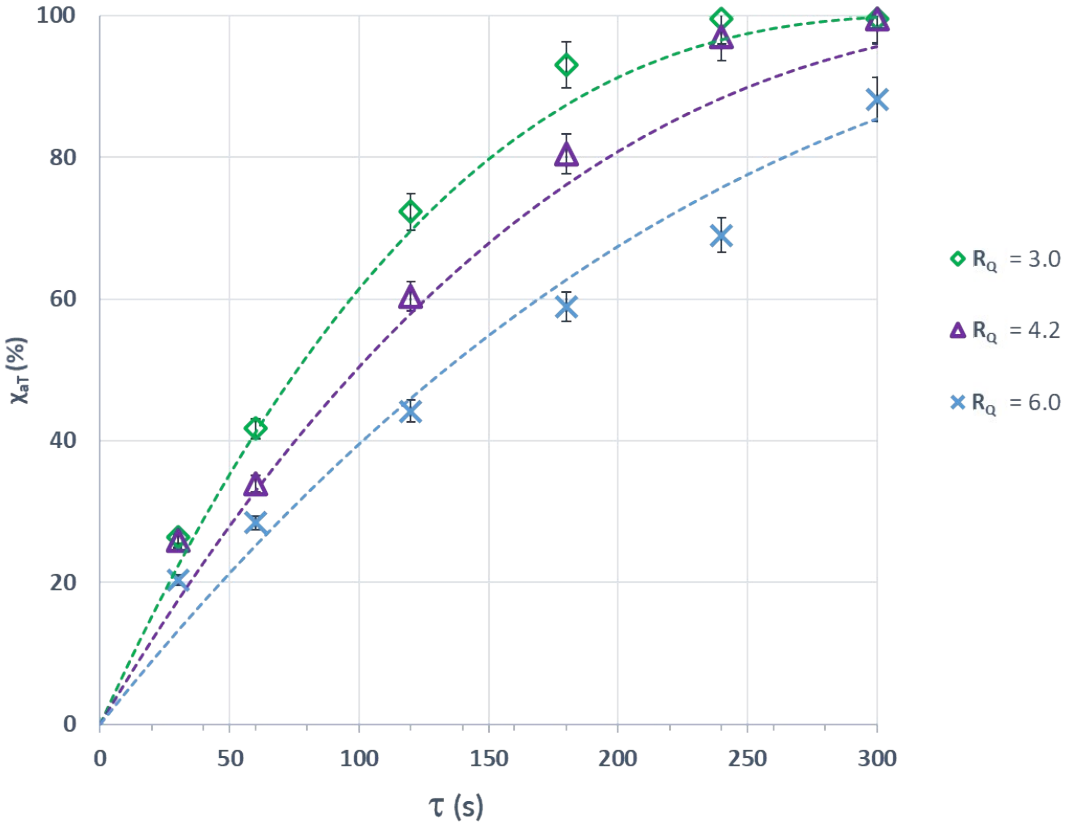

Figure S16: Conversion of α-terpinene, $\chi_{\alpha T}$, versus residence time, τ, for RB solubilized in ethanol for three volumetric ratio, R_Q. The conversions predicted by the model (Eq. 9) are shown as dotted lines for each volumetric ratio. (Operating conditions: C_{RB} = 6.10^{-6} mol.L^{-1}; $C_{\alpha T,0}$ = 3.10^{-2} mol.L^{-1}; f = 1.21 ± 0.02; q_r = 1668 µmol$_{h\upsilon}$.m^{-2}.s^{-1})

Volumetric ratio, R_Q	Conversion (%)						Yield (%)					
	30 s	60 s	120 s	180 s	240 s	300 s	30 s	60 s	120 s	180 s	240 s	300 s
3	26.4 ± 0.9	41.7 ± 1.5	72.3 ± 2.5	93.9 ± 3.3	99.5 ± 3.5	99.6 ± 3.5	19.2 ± 0.7	34.1 ± 1.2	59.5 ± 2.1	77.9 ± 2.7	82.6 ± 2.9	81.4 ± 2.9
4.2	25.9 ± 0.9	34.0 ± 1.2	60.4 ± 2.1	80.5 ± 2.8	97.1 ± 3.4	99.5 ± 3.5	15.8 ± 0.6	27.8 ± 1.0	50.8 ± 1.8	70.2 ± 2.5	86.2 ± 3.0	86.3± 3.0
6	20.3 ± 0.7	28.4 ± 1.0	44.2 ± 1.6	58.9 ± 2.1	69.0 ± 2.4	88.2 ± 3.1	12.1 ± 0.4	19.6 ± 0.7	33.9 ± 1.2	47.2 ± 1.7	56.2 ± 2.0	72.4 ± 2.5

Table S5: Conversion of α-terpinene and yield of ascaridole for 3 volumetric ratio and different residence times (see **Figure S16**)

Table S6: Selectivity and photobleaching yield for 3 volumetric ratio and different residence times (see **Figure S16**)

Volumetric ratio, R_Q	**Selectivity**						**Photobleaching yield (%)**					
	30 s	**60 s**	**120 s**	**180 s**	**240 s**	**300 s**	**30 s**	**60 s**	**120 s**	**180 s**	**240 s**	**300 s**
3	72.8 ± 2.5	82.0 ± 2.9	82.3 ± 2.9	83.0 ± 2.9	83.0 ± 2.9	81.7 ± 2.9	4.6 ± 0.1	1.5 ± 0.1	1.5 ± 0.1	6.1 ± 0.2	6.2 ± 0.2	7.6 ± 0.2
4.2	61.3 ± 2.1	81.8 ± 2.9	84.1 ± 2.9	87.3 ± 3.1	88.8 ± 3.1	86.8 ± 3.0	5.0 ± 0.1	5.0 ± 0.1	5.0 ± 0.1	3.3 ± 0.1	1.7 ± 0.1	3.3 ± 0.1
6	60.0 ± 2.1	69.0 ± 2.4	76.6 ± 2.7	80.2 ± 2.8	81.5 ± 2.9	82.1 ± 2.9	2.9 ± 0.1	1.5 ± 0.1	1.5 ± 0.1	2.9 ± 0.1	5.8 ± 0.2	4.4 ± 0.1

S11.b *Illustration of the Taylor flows with different volumetric ratio*

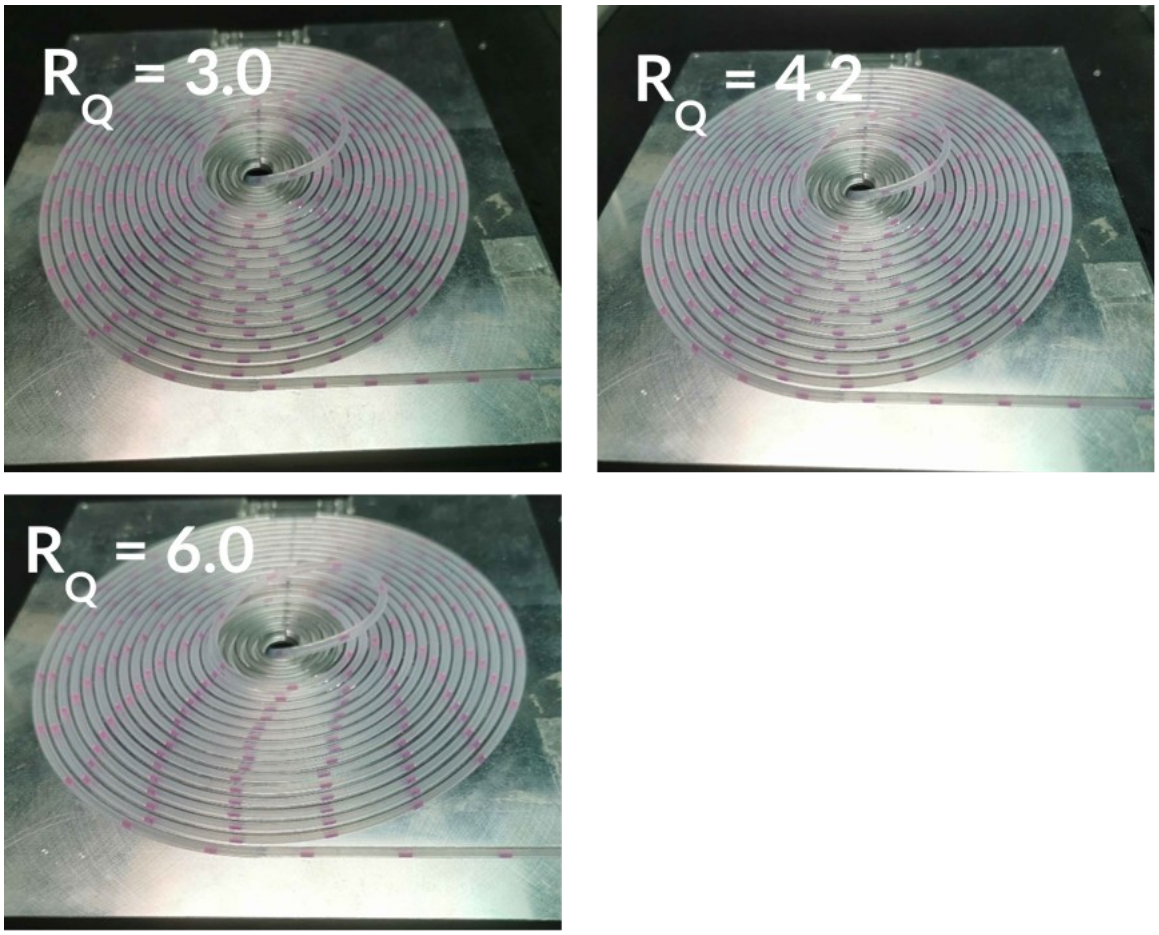

Figure S17 : Typical images of the Taylor flows for different volumetric ratio, R_Q

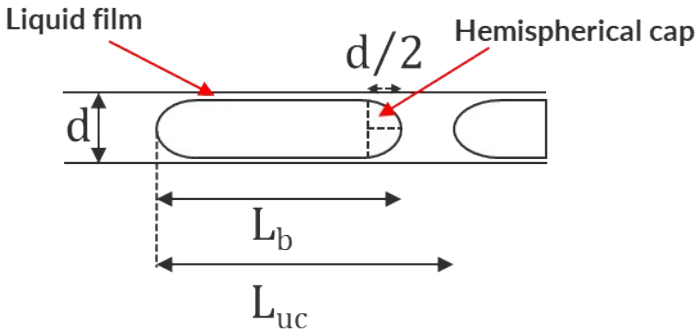

S11.c *Experimental demonstration of the proportionality between the interfacial area and* $\frac{1}{1+R_Q}$

Scheme S1:Schematic representation of the Taylor flow in the FEP tube with inner diameter, *d*. L_b (m) is the length of a bubble and L_{uc} (m) the unit cell length. It is assumed that the bubbles could be described as two hemispherical caps for the bubble nose and rear (with a diameter equal to *d*), and with a cylindrical shape for the bubble body which length equals to (L_b-*d*).

Bubbles and liquid slugs were measured by image processing (**Table S7**).

Table S7 *: Flow characteristics for different volumetric ratios* (R_Q)

R_Q	C_{aT} (mol.L^{-1})	Q_L (mL.min^{-1})	Q_G (mL.min^{-1})	L_{slug} (cm)	L_b (cm)	a_f (m^{-1})	a_c (m^{-1})	a (m^{-1})
3.0	0.022	0.320	0.97	0.40	1.21	2760	**248**	3008
4.2	0.030	0.250	1.05	0.39	1.74	3082	**188**	3271
6.0	0.044	0.185	1.12	0.44	2.82	3342	**123**	3464

From these measurements, the interfacial area *a* (m^{-1}) could be calculated as follows:

$$a = a_f + a_c = \frac{S_f}{V_{uc}} + \frac{S_c}{V_{uc}} \qquad (Eq.\,S12)$$

With a_f (m^{-1}) the interfacial area related to the lubrication film between the bubble and the tubing wall and a_c (m^{-1}) the interfacial area related to the bubble's rear and nose (see **Scheme S1**).

$$V_{uc} = L_{uc} \times \frac{\pi d^2}{4} \qquad (Eq.\,S13)$$

$$S_f = \pi d(L_b - d) \qquad (Eq.\,S14)$$

$$S_c = \pi d^2 \qquad (Eq.\,S15)$$

With V_{uc} (m^3), the unit cell volume, S_f (m^2) the film surface and S_c (m^2) the cap surface. According to these previous equations, the interfacial area could therefore be described as:

$$a = \frac{4(L_b - d)}{d\,L_{uc}} + \frac{4}{L_{uc}} \qquad (Eq.\,S16)$$

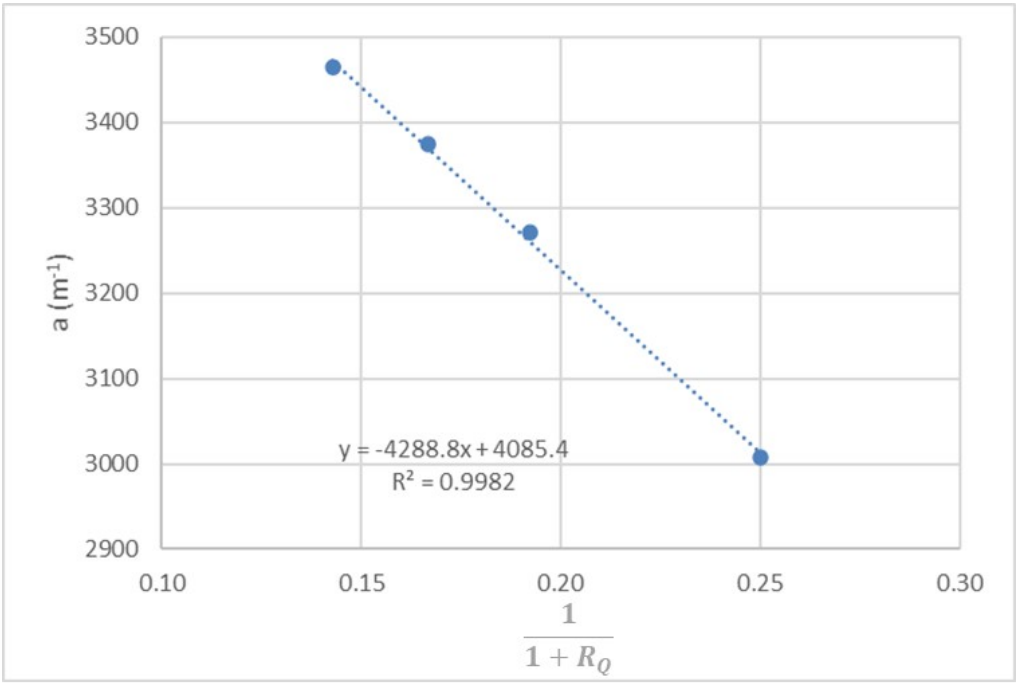

Figure S18 shows that the experimental interfacial area is proportional to $\frac{1}{1+R_Q}$

Figure S18 : Variation of interfacial area as a function of $\frac{1}{1+R_Q}$

S11.d *Theoretical demonstration of the proportionality between the interfacial area and* $\frac{1}{1+R_Q}$

This proportionality can be also demonstrated theoretically

$$\epsilon_L = \frac{V_L}{V_L + V_G} \sim \frac{N_{slug} \times V_{slug}}{V} \qquad (Eq.S17)$$

Where ϵ_L(-) is the liquid retention, V_L (m^3) the liquid volume, V_G (m^3) the gas volume, V_{slug} (m^3) the slug volume and N_{slug} the number of slugs, or bubbles.

Neglecting the slip velocity between the gas and liquid phases, we can write

$$\epsilon_L \sim \frac{Q_L}{Q_L + Q_G} = \frac{Q_L/Q_G}{(Q_L + Q_G)/Q_G} = \frac{1/R_Q}{1 + 1/R_Q} = \frac{1}{1+R_Q} \qquad (Eq.S18)$$

With Q_L *and* Q_G ($mL.min^{-1}$) liquid and gas flow rates respectively. From this, we can deduce:

$$\frac{1}{1+R_Q} = \frac{N_{slug} \times V_{slug}}{V} \qquad (Eq.S19)$$

$$V = N_{slug} \times V_{slug}\,(1 + R_Q) \qquad (Eq.S20)$$

So, by referring back to the definition of interfacial area (exchange surface offered by all the bubbles per unit volume), we can demonstrate its proportionality to $\frac{1}{1+R_Q}$

$$a = \frac{S_{bubbles}}{V} = \frac{N_{slug} \times S_{1\,bubble}}{N_{slug} \times V_{slug}(1+R_q)} = \frac{S_{1\,bubble}}{V_{slug}} \times \frac{1}{1+R_Q} \propto \frac{1}{1+R_Q} \qquad (Eq.S21)$$

S11.e *Mass balance on the oxygen dissolved in the liquid phase*

The writing of the **mass balance on the oxygen** in the liquid phase accounts for the consumption of oxygen by the photooxygenation (expressed here as a second-order law for simplicity purpose), and for the oxygen flux coming from the bubbles. The latter depends on the overall volumetric mass transfer coefficient, $k_L a$ (i.e. the product between the liquid-side mass transfer coefficient, k_L, and the interfacial area, a), on the concentration in dissolved oxygen at saturation, $C_{O_2}^{*}$, and on the enhancement factor, E, which is a function of the Hatta number. Thus, assuming a plug-flow behaviour, one can write:

$$\frac{dC_{O2}}{d\tau} = -kC_{RB}C_{O_2} + k_L a E\left(C_{O_2}^{*} - C_{O_2}\right) \qquad (Eq.S22)$$

If we consider a steady state for the oxygen (i.e. a constant dissolved oxygen concentration whatever the residence time), and that the oxygen concentration in the bulk is negligible towards the one at saturation ($C_{O_2}^{*}$), the dioxygen concentration, C_{O_2}, becomes proportional to $k_L a$. Considering that the liquid-side mass transfer coefficient, k_L, remains almost constant whatever R_Q, the oxygen concentration, C_{O_2}, is then proportional to the interfacial area a, and thus, as demonstrated previously, to $\frac{1}{1+R_Q}$.

S11.e *Rescaling the kinetic curves for different volumetric ratios*

Finally, following the previous demonstrations, it is possible to rescale the previous results

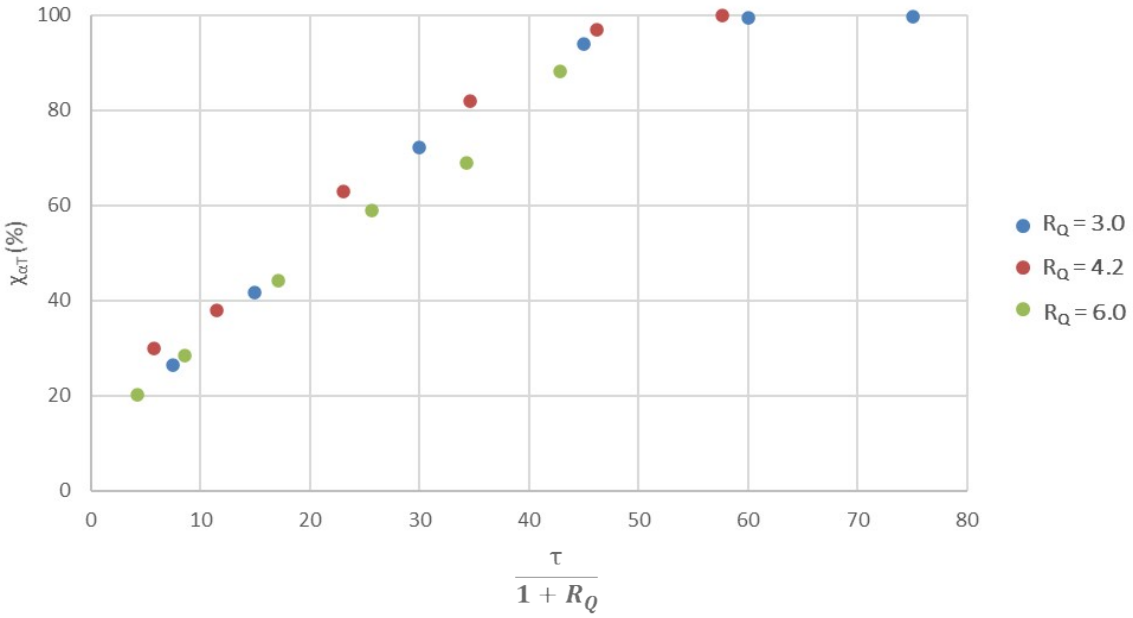

(**Figure S16**) as shown in **Figure S19**.

Figure S19: Conversion of α-terpinene, $\chi_{\alpha T}$, versus $\frac{\tau}{1+R_Q}$ for various volumetric ratio

S.12 Procedure to test the reusability of the photoactive colloids

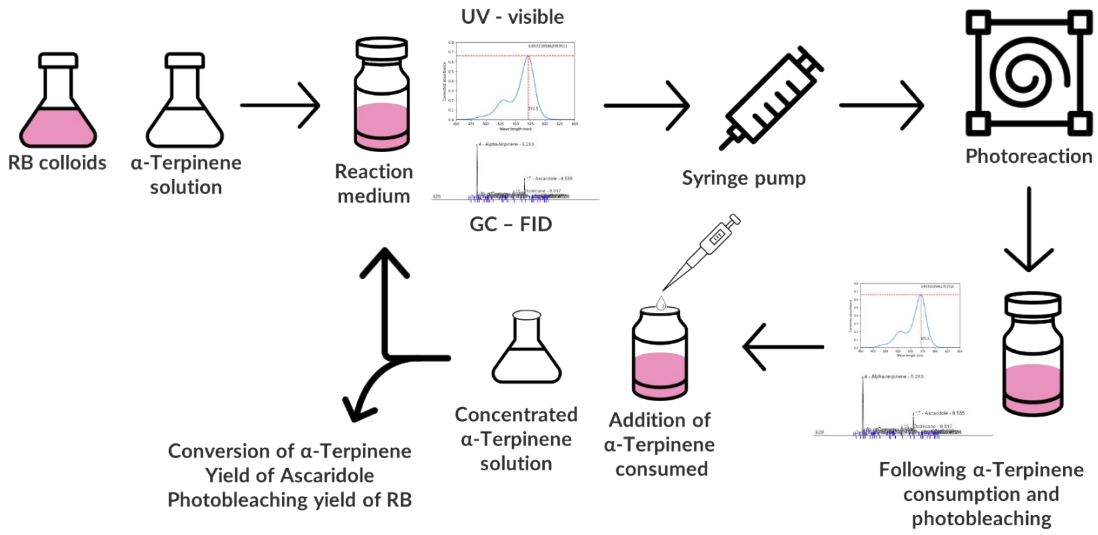

Figure S20: Protocol to test the reusability of the colloids

Following the protocol presented in **Figure S20**, this set of experiments was carried out in a total volume of 50 mL with a residence time of 60 s, allowing a cycle to be completed in just over an hour. The same reaction medium, i.e. the initial 50 mL, was used for all the cycles, without replenishing the volume loss for analysis, i.e. around 2 mL. It was thus important to use a volume widely higher than the desired volume loss in each cycle, in order to keep an almost identical reaction medium at the start of each cycle.

Each cycle began with a GC-FID and UV analysis to precisely determine the amount of α-terpinene and RB in the reaction medium. For each experiment, the reactor was run for three residence times before sample's collection to achieve steady-state flow conditions. Then, the cycle was started and the reactor won't be shut down until the 50 mL has elapsed.

The general operating conditions for each cycle were: τ = 60 s; Q_L = 0.75 mL.min^{-1}; Q_G = 3.2 mL.min^{-1}; C_{RB} = 6.10^{-6} mol.L^{-1}; $C_{\alpha T,0}$ = 3.10^{-2} mol.L^{-1}; R_Q = 4.26 ± 0,06; f = 1.21 ± 002; q_r = 1668 µmol$_{h\upsilon}$.m^{-2}.s^{-1}.

At the end of the cycle, conversion in α-terpinene, noted $\chi_{\alpha T}$ (-), was analysed by gas chromatography coupled to an FID detector using dodecane as an internal standard, and yield of ascaridole and selectivity were also determined. Once the conversion was determined, the amount of α-terpinene consumed was replaced by the same amount from a concentrated α-terpinene solution (85 $g.L^{-1}$) to start the next cycle with an identical initial amount of α-terpinene. The photobleaching yield of RB, χ_{RB} (-) was calculated as the ratio of the absorbances at λ_{max} after the cycle to the absorbance at the same wavelength before the cycle. The RB concentration was not adjusted for each cycle, as the aim here was to see how robust the RB was over time. At this point, the reaction medium was ready to be reintroduced into the reactor for the next cycle.

S.13 Photosensitizer cyclability results with soluble Rose Bengal

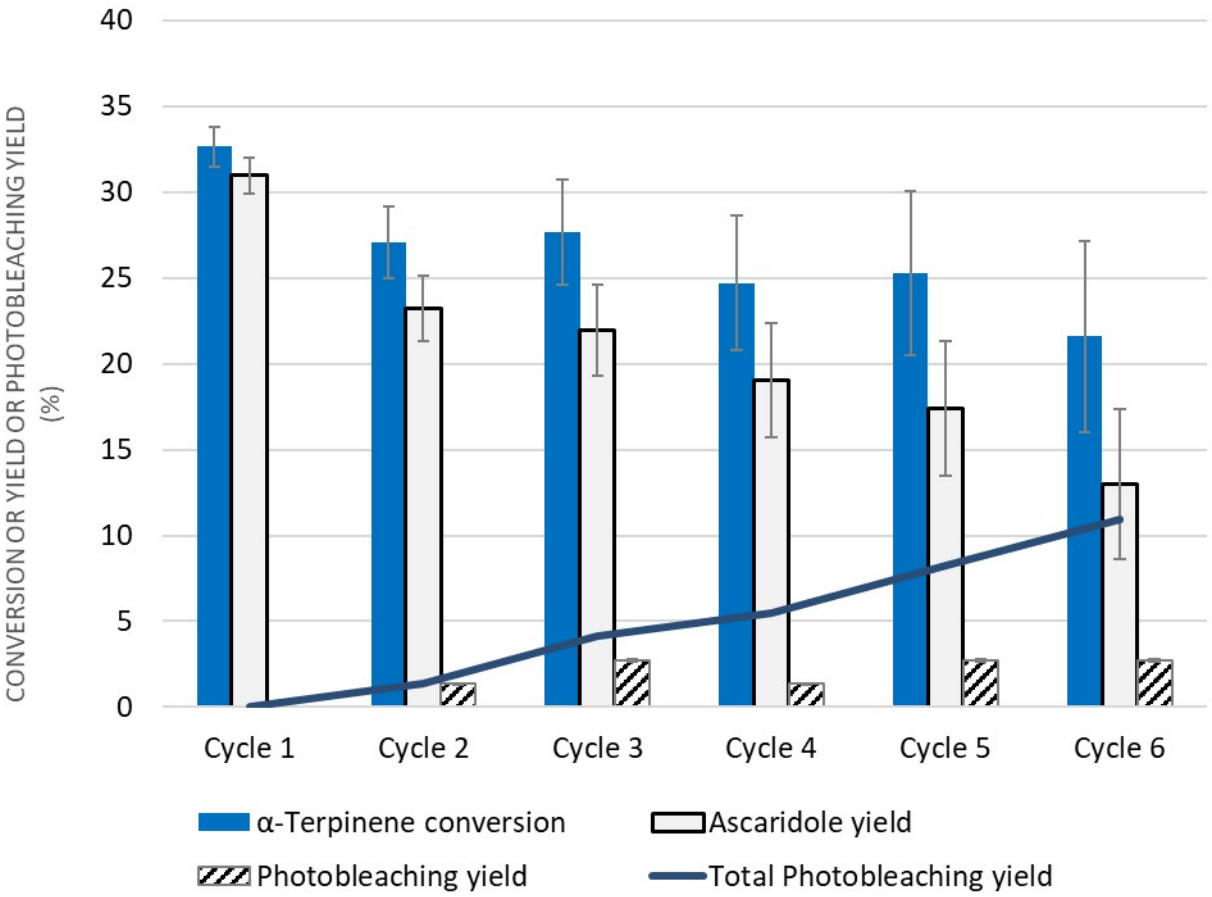

Figure S21: Conversion of α-terpinene, yield of ascaridole, and photobleaching yield RB solubilized in ethanol for 6 cycles of experiments, (operating conditions: τ = 60 s; Q_L= 0.75 mL.min^{-1}; Q_G = 3.2 mL.min^{-1}; C_{RB} = 6.10^{-6} mol.L^{-1}; $C_{\alpha T,0}$ = 3.10^{-2} mol.L^{-1}; R_Q = 4.26 ± 0,06; f= 1.21 ± 0.02; q_r= 1668 µmol$_{h\upsilon}$.m^{-2}.s^{-1})

S.14 Initial reaction rates

The initial reaction rates, noted $\Gamma_{0,}$ were calculated from the initial slope of the curves relating the variation of the conversion in alpha-terpinene with the residence times.

Table S8 : Initial reaction rates, noted $\Gamma_{0,}$ for different operating conditions: soluble RB or RB@CSLP$_{66/2.0,}$ photon flux densities of 976 or 1668 $\mu mol_{h\upsilon}.m^{-2}.s^{-1}$

	RB type	**C_{RB} ($\mu mol.L^{-1}$)**	**q_r ($\mu mol_{h\upsilon}.m^{-2}.s^{-1}$)**	**Γ_0 (s^{-1})**
Entry 1	Soluble	0.1	1668	0.04
Entry 2	Soluble	1.5	1668	0.10
Entry 3	Soluble	3	1668	0.24
Entry 4	Soluble	5	1668	0.35
Entry 5	Soluble	6	1668	0.49
Entry 6	Soluble	12	1668	0.97
Entry 7	Soluble	5	976	0.20
Entry 8	RB@CSLP$_{66/2.0}$	3	1668	0.22
Entry 9	RB@CSLP$_{66/2.0}$	6	1668	0.49
Entry 10	RB@CSLP$_{66/2.0}$	12	1668	0.84
Entry 11	RB@CSLP$_{66/2.0}$	5	976	0.27

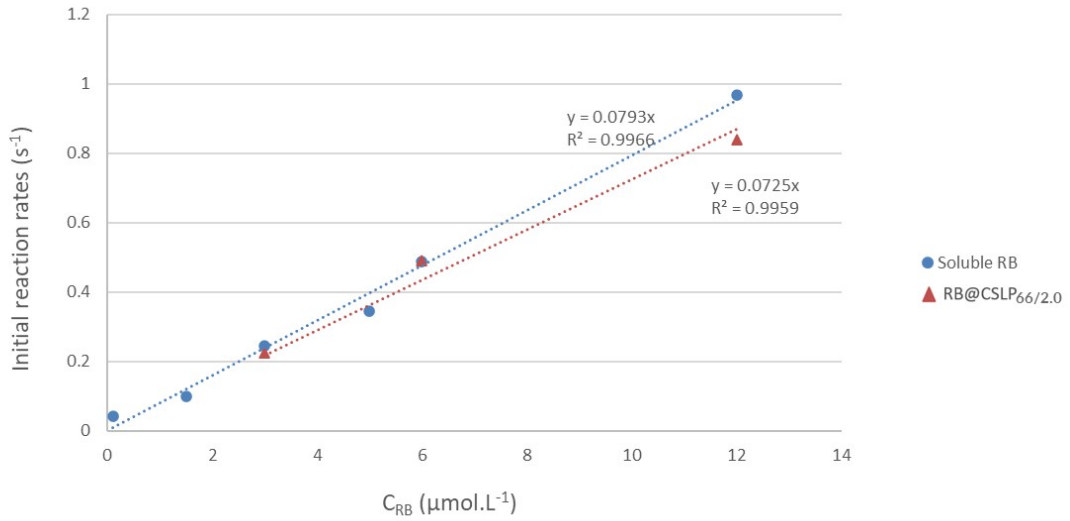

- *Effect of the RB concentration*

Figure S22: Initial reaction rates, $\Gamma_{0,}$ of the different operating conditions (soluble RB or RB@CSLP$_{66/2.0}$, photon flux densities of 976 or 1668 µmol$_{h\upsilon}$.m^{-2}.s^{-1}) as a function of the molar concentration of RB in µmol.L^{-1}

- *Effect of the photon flux densities*

The comparison of Entries 5 and 7 (soluble RB with C_{RB}=5 µM) showed that the ratio of the initial reaction rates Γ_0 obtained for both photon flux densities (all the other parameters being kept constant) was found equal to the ratio of the two incident photon fluxes (1.76 *vs* 1.71).

S.15 Writing of the representation model

The photooxygenation is a function of the concentration in reactants: $C_{\alpha T}$ the concentration in α-terpinene, C_{RB} the concentration in RB, q_r the photon flux density flux of photon, $C_{O_2}$the concentration in oxygen. This last concentration was shown to be proportional to interfacial area, and thus to $\frac{1}{1+R_Q}$. Following these assumptions, the consumption of $C_{\alpha T}$ can be written as:

$$\frac{dC_{\alpha T}}{d\tau} = -k\frac{{C_{\alpha T}}^n C_{RB}\, q_r}{1+R_Q} \qquad (Eq.S23)$$

where *k* is an empirical constant and n is the order of the reaction.

The conversion of the $C_{\alpha T}$ is defined as:

$$\chi_{\alpha T} = 1 - \frac{C_{\alpha T}}{C_{\alpha T,0}} \qquad (Eq.S24)$$

- **If n = 1**

$$\chi_{\alpha T} = 1 - e^{-k\frac{C_{RB}\, q_r}{1+R_Q}\tau} \qquad (Eq.S25)$$

The results are shown below in **Figure S23**.

- **If n ≠ 1:**

$$C_{\alpha T} = \left({C_{\alpha T}}_0^{1-n} - (1-n)k\frac{C_{RB}\, q_r}{1+R_Q}\tau\right)^{\frac{1}{1-n}} \qquad (Eq.S26)$$

The results are shown below in **Figures 2, 3, S15 and S16.** The fitting is better with n ≠ 1.

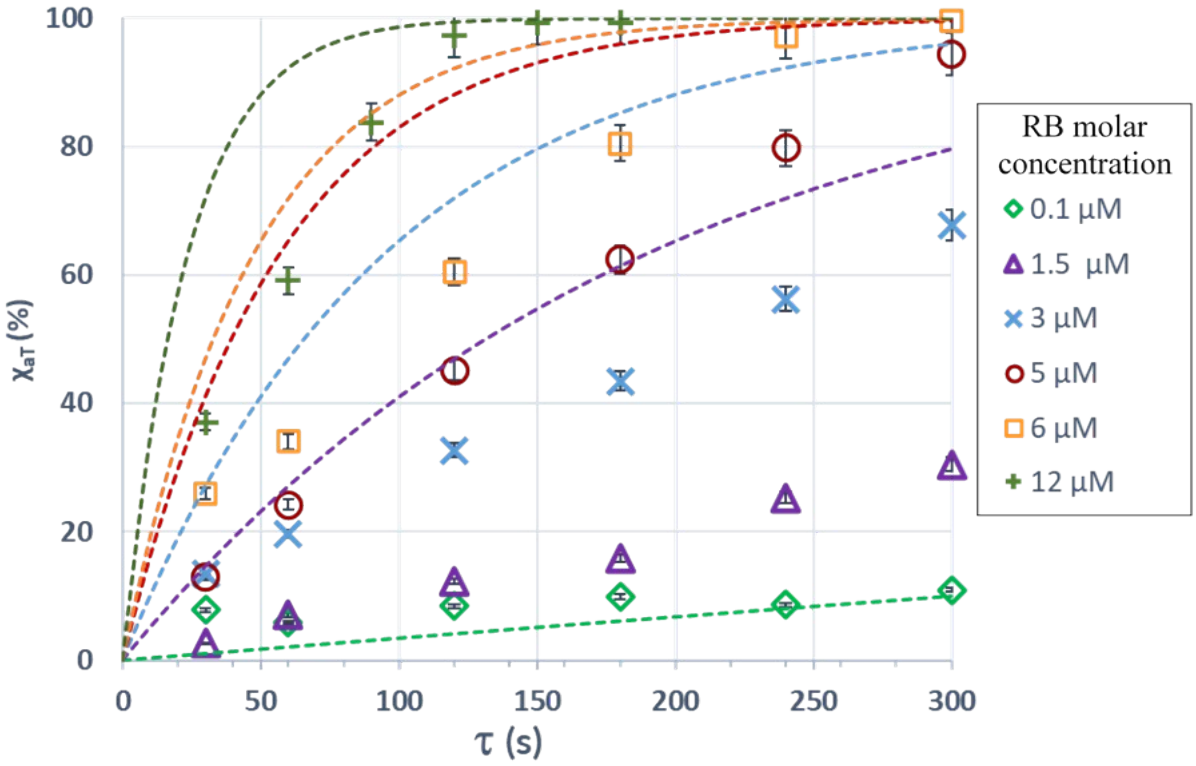

Figure S23 : Conversion of α-terpinene, $\chi_{\alpha T}$, versus residence time, τ, for different RB molar concentrations using soluble RB in ethanol. The conversions predicted by the kinetic model for an order of the reaction n=1 (Eq. S25) are shown as dotted lines for each RB concentration Operating conditions: $C_{\alpha T,0} = 3.10^{-2}$ mol.L^{-1}; $R_Q = 4.26 \pm 0.06$; $f = 1.21 \pm 0.02$; $q_r = 1668$ µmol $_{h\upsilon}$.m^{-2}.s^{-1}.

The code used for experiment fitting (conversion versus residence time) with a kinetic model is available below:

https://github.com/bacchin/chemical_engineering_python/blob/master/rech/fit_photoconversion.ipynb

S.16 Conversion, yield, selectivity and photobleaching yield of Figure 2

Table S9: Conversion of α-terpinene and yield of ascaridole soluble RB at different molar concentrations and residence times (see **Figure 2**)

C_{RB} (µM) (Molar percents)	Conversion (%)						Yield (%)					
	30 s	**60 s**	**120 s**	**180 s**	**240 s**	**300 s**	**30 s**	**60 s**	**120 s**	**180 s**	**240 s**	**300 s**
0.1 ($3.3.10^{-4}$ mol %)	7.8 ± 0.3	5.9 ± 0.2	8.5 ± 0.3	9.9 ± 0.4	8.6 ± 0.3	11.0 ± 0.4	0.2 ± 0.1	0.9 ± 0.1	4.1 ±0.1	3.1 ± 0.1	2.8 ± 0.1	3.6 ± 0.1
1.5 (5.10^{-3} mol %)	2.7 ± 0.1	7.0 ± 0.3	12.3 ± 0.4	15.8 ± 0.6	25.3 ± 0.9	30.5 ± 1.1	3.7 ± 0.1	6.3 ± 0.2	12.3 ± 0.4	17.1 ± 0.6	21.4 ± 0.8	23.7 ± 0.8
3 (1.10^{-2} mol %)	13.4 ± 0.5	19.7 ± 0.7	32.7 ± 1.1	43.5 ± 1.5	56.3 ± 2.0	67.8 ± 2.4	8.6 ± 0.3	14.4 ± 0.5	25.5 ± 0.9	35.8 ± 1.3	46.2 ± 1.6	58.2 ± 2.0
5 ($1.7.10^{-2}$ mol %)	12.9 ± 0.5	24.2 ± 0.9	45.1 ± 1.3	62.4 ± 2.2	79.8 ± 2.8	94.4 ± 3.3	14.3 ± 0.5	23.6 ± 0.8	41.8 ± 1.5	57.7 ± 2.0	74.1 ± 2.6	86.9 ± 3.0
6 (2.10^{-2} mol %)	25.9 ± 0.9	34.0 ± 1.2	60.4 ± 2.1	80.5 ± 2.8	97.1 ± 3.4	99.5 ± 3.5	15.8 ± 0.6	27.8 ± 1.0	50.8 ± 1.8	70.2 ± 2.5	86.2 ± 3.0	86.3 ± 3.0
C_{RB} (µM) (Molar percents)	**30 s**	**60 s**	**90 s**	**120 s**	**150 s**	**180 s**	**30 s**	**60 s**	**90 s**	**120 s**	**150 s**	**180 s**
12 (4.10^{-2} mol %)	37.1 ± 1.3	59.1 ± 2.1	83.7 ± 2.9	97.3 ± 3.4	99.3 ± 3.5	99.4 ± 3.5	28.7 ± 1.0	43.2 ± 1.5	65.7 ± 2.3	81.6 ± 2.9	74.3 ± 2.6	85.7 ± 3.0

The mol % reported corresponds the ratio between the RB and α-terpinene molar concentrations.

Table S10: Selectivity and photobleaching yield for soluble RB at different molar concentrations and residence times (see **Figure 2**)

C_{RB} (µM) (Molar percents)	Selectivity						Photobleaching yield (%)					
	30 s	**60 s**	**120 s**	**180 s**	**240 s**	**300 s**	**30 s**	**60 s**	**120 s**	**180 s**	**240 s**	**300 s**
0.1 ($3.3.10^{-4}$ mol %)	ND	ND	ND	ND	ND	ND	ND	ND	ND	ND	ND	ND
1.5 (5.10^{-3} mol %)	ND	89.7 ± 3.1	100 ± 3.5	100 ± 3.5	84.4 ± 3.0	77.7 ± 2.7	0	0	0	0	0	0
3 (1.10^{-2} mol %)	63.7 ±3.2	73.3 ± 2.6	77.9 ± 2.7	82.4 ± 2.9	82.1 ± 2.9	85.9 ± 3.0	0	0	0	0	3.5 ± 0.1	3.5 ± 0.1
5 ($1.7.10^{-2}$ mol %)	ND	97.5 ± 3.4	92.6 ± 3.2	92.4 ± 3.2	93.0 ± 3.3	92.0 ± 3.2	1.9 ± 0.1	1.9 ± 0.1	3.7 ± 0.1	3.7 ± 0.1	5.6 ± 0.1	5.6 ± 0.1
6 (2.10^{-2} mol %)	61.3 ±3.0	81.8 ± 2.9	84.1 ± 2.9	87.3 ± 3.1	88.8 ± 3.1	86.8 ± 3.2	5.0 ± 0.1	5.0 ± 0.1	5.0 ± 0.1	3.3 ± 0.1	1.7 ± 0.1	3.3 ± 0.1
C_{RB} (µM) (Molar percents)	**30 s**	**60 s**	**90 s**	**120 s**	**150 s**	**180 s**	**30 s**	**60 s**	**90 s**	**120 s**	**150 s**	**180 s**
12 (4.10^{-2} mol %)	77.4 ± 2.7	73.2 ± 2.6	78.5 ± 2.7	83.8 ± 2.9	74.8 ± 2.6	86.3 ± 3.0	0.7 ± 0.1	0	0	0.7 ± 0.1	0	0.7 ± 0.1

The mol % reported corresponds the ratio between the RB and α-terpinene molar concentrations.

S.17 Conversion, yield, selectivity and photobleaching yield of Figure 3

Table S11: Conversion of α-terpinene and yield of ascaridole various colloidal samples and soluble RB at 6 µmol.L^{-1}(see **Figure 3**)

Sample	Conversion (%)						Yield (%)					
	30 s	60 s	120 s	180 s	240 s	300 s	30 s	60 s	120 s	180 s	240 s	300 s
RB@CSLP$_{122/2.1}$	21.3 ± 0.8	33.4 ± 1.2	54.3 ± 1.9	75.1 ± 2.6	93.8 ± 3.3	99.4 ±3.5	17.0 ± 0.6	31.3 ± 1.1	45.2 ± 1.6	63.5 ± 2.2	81.0 ± 2.8	82.0 ± 2.9
RB@CSLP$_{66/2.0}$	18.5 ± 0.7	33.1 ± 1.2	53.7 ± 1.9	73.4 ± 2.6	91.3 ± 3.2	98.0 ± 3.4	16.1 ± 0.6	27.2 ± 1.0	45.7 ± 1.6	63.0 ± 2.2	85.3 ± 3.0	77.5 ± 2.7
RB@CSLP$_{162/3.4}$	18.0 ± 0.6	30.4 ± 1.1	53.3 ± 1.9	72.5 ± 2.5	92.3 ± 3.2	98.5 ± 3.5	18.8 ± 0.7	29.3 ± 1.0	44.8 ± 1.6	65.1 ± 2.3	80.7 ± 2.8	82.3 ± 2.9
RB@CSLP$_{112/1.1}$	20.5 ± 0.7	35.2 ± 1.2	57.1 ± 2.0	76.6 ± 2.7	94.1 ± 3.3	97.7 ± 3.4	13.9 ± 0.5	24.2 ± 0.9	44.2 ± 1.6	61.9 ± 2.2	75.8 ± 2.7	76.2 ± 2.7
RB@CSLP$_{167/0.68}$	21.5 ± 0.8	36.4 ± 1.3	58.4 ± 2.0	80.2 ± 2.8	95.6 ± 3.3	96.3 ± 3.4	17.6 ± 0.6	25.7 ± 0.9	48.7 ± 1.7	66.1 ± 2.3	74.2 ± 2.6	71.9 ± 2.5
RB@CSLP$_{257/0.21}$	14.9 ± 0.5	20.6 ± 0.7	40.3 ± 1.4	61.7 ± 2.2	75.8 ± 2.7	88.1 ± 3.1	12.8 ± 0.5	17.7 ± 0.6	27.6 ± 1.0	40.2 ± 1.4	45.1 ± 1.6	60.9 ± 2.1
Soluble RB	25.9 ± 0.9	34.0 ± 1.2	60.4 ± 2.1	80.5 ± 2.8	97.1 ± 3.4	99.5 ± 3.5	15.8 ± 0.6	27.8 ± 1.0	50.8 ± 1.8	70.2 ± 2.5	86.2 ± 3.0	86.3 ± 3.0

Table S12: Selectivity and photobleaching yield for various colloidal samples and soluble RB at 6 µmol.L^{-1}(see **Figure 3**)

Sample	Selectivity						Photobleaching yield (%)					
	30 s	60 s	120 s	180 s	240 s	300 s	30 s	60 s	120 s	180 s	240 s	300 s
RB@CSLP$_{122/2.1}$	79.7 ± 2.8	94.0 ± 3.3	83.3 ± 2.9	84.6 ± 3.0	86.3 ± 3.0	82.5 ± 2.9	1.5 ± 0.1	1.5 ± 0.1	3.0 ± 0.1	4.6 ± 0.1	4.6 ± 0.1	4.6 ± 0.1
RB@CSLP$_{66/2.0}$	86.7 ± 3.0	82.2 ± 2.9	85.0 ± 3.0	85.9 ± 3.0	93.5 ± 3.3	79.1 ± 2.8	1.5 ± 0.1	1.5 ± 0.1	3.1 ± 0.1	4.6 ± 0.1	7.7 ± 0.2	12.3 ± 0.3
RB@CSLP$_{162/3.4}$	ND	96.4 ± 3.4	84.2 ± 2.9	89.8 ± 3.1	87.5 ± 3.1	83.6 ± 2.9	3.2 ± 0.1	3.2 ± 0.1	4.8 ± 0.1	6.4 ± 0.2	6.4 ± 0.2	8.0 ± 0.2
RB@CSLP$_{112/1.1}$	67.7 ± 2.4	68.7 ± 2.4	77.4 ± 2.7	80.9 ± 2.8	80.6 ± 2.8	78.0 ± 2.7	4.5 ± 0.1	3.0 ± 0.1	4.5 ± 0.1	7.5 ± 0.2	9.0 ± 0.2	9.0 ± 0.2
RB@CSLP$_{167/0.68}$	81.9 ± 2.9	70.6 ± 2.5	83.5 ± 2.9	82.5 ± 2.9	77.6 ± 2.7	74.6 ± 2.6	ND	ND	ND	ND	ND	ND
RB@CSLP$_{257/0.21}$	85.6 ± 3.0	86.1 ± 3.0	68.6 ± 2.4	65.5 ± 2.3	59.5 ± 2.1	69.1 ± 2.4	ND	ND	ND	ND	ND	ND
Soluble RB	61.3 ± 2.1	81.8 ± 2.9	84.1 ± 2.9	87.3 ± 3.1	88.8 ± 3.1	86.8 ± 3.0	5.0 ± 0.1	5.0 ± 0.1	5.0 ± 0.1	3.3 ± 0.1	1.7 ± 0.1	3.3 ± 0.1

References

(1) Boussiron, C.; Le Bechec, M.; Sabalot, J.; Lacombe, S.; Save, M. Photoactive Rose Bengal-Based Latex *via* RAFT Emulsion Polymerization-Induced Self-Assembly. *Polym. Chem.* **2021**, *12* (1), 134–147. https://doi.org/10.1039/D0PY01128B.

(2) Mei, M; Felis, F.; Hébrard, G.; Dietrich, N.; Loubière, K. Hydrodynamics of Gas–Liquid Slug Flows in a Long In-Plane Spiral Shaped Milli-Reactor. *Theor. Found. Chem. Eng.* **2020**, *54* (1), 25–47. https://doi.org/10.1134/S0040579520010169.

(3) Radjagobalou, R.; Blanco, J.-F.; Petrizza, L.; Le Bechec, M.; Dechy-Cabaret, O.; Lacombe, S.; Save, M.; Loubiere, K. Efficient Photooxygenation Process of Biosourced α-Terpinene by Combining Controlled LED-Driven Flow Photochemistry and Rose Bengal-Anchored Polymer Colloids. *ACS Sustain. Chem. Eng.* **2020**, *8* (50), 18568–18576. https://doi.org/10.1021/acssuschemeng.0c06627.

(4) Radjagobalou, R.; Dias da Silva Freitas, V.; Blanco, J.-F.; Gros, F.; Dauchet, J.; Cornet, J.-F.; Loubière, K. A Revised 1D Equivalent Model for the Determination of Incident Photon Flux Density in a Continuous-Flow LED-Driven Spiral-Shaped Microreactor Using the Actinometry Method with Reinecke's Salt. *J. Flow Chem.* **2021**, *11*, 357–367. https://doi.org/10.1007/s41981-021-00179-w.